Proceedings of the ASME 2021
International Design Engineering Technical Conferences and
Computers and Information in Engineering Conference
IDETC/CIE 2021
August 17 – 20, 2021, Virtual Conference

DETC2021-69977

NUMERICAL ANALYSIS AND PARAMETER OPTIMIZATION OF A PORTABLE TWO-BODY ATTENUATOR WAVE ENERGY CONVERTER

Joseph Capper, Jia Mi, Qiaofeng Li, Lei Zuo*

Department of Mechanical Engineering, Virginia Tech, Blacksburg, VA, 24061, USA (leizuo@vt.edu)

ABSTRACT

Easily portable, small-sized ocean wave energy converters (WECs) may be used in many situations where large-sized WEC devices are not necessary or practical. Power maximization for small-sized WECs amplifies challenges that are not as difficult with large-sized devices, especially tuning the device's natural frequency to match the wave frequency and achieve resonance. In this study, power maximization is performed for a small-sized, two-body attenuator WEC with a footprint constraint of about Im. A thin, submerged tuning plate is added to each body to increase added mass without significantly increasing hydrostatic stiffness in order to reach resonance. Three different body crosssection geometries are analyzed. Device power absorption is determined through time domain simulations using WEC-Sim with a simplified two-degree-of-freedom (2DOF) model and a more realistic three-degree-of-freedom (3DOF) model. Different drag coefficients are used for each geometry to explore the effect of drag. A mooring stiffness study is performed with the 3DOF model to investigate the mooring impact. Based on the 2DOF and 3DOF power results, there is not a significant difference in power between the shapes if the same drag coefficient is used, but the elliptical shape has the highest power after assigning a different approximate drag coefficient to each shape. The mooring stiffness study shows that mooring stiffness can be increased in order to increase relative motion between the two bodies and consequently increase the power.

Keywords: Wave Energy Converter (WEC), Attenuator, Geometry Optimization, Resonance Tuning, Power Maximization

1. INTRODUCTION

Ocean wave energy shows major promise as a clean, abundant, and renewable source of energy with a strategic location in close proximity to global population centers. Presently, around 60% of the world's population lives in coastal regions [1], including 40% living within 20 km of the coast [2],

and those percentages are expected to increase as cities grow. Globally, usable wave energy has been estimated at over 2 TW [3]. In the United States alone, wave energy could provide 2,640 TWh/yr, which is about 2/3 of the electricity annually consumed in the U.S. [4]. Today, there is enormous diversity in the different types of wave energy converters (WECs), with no convergence on a widely accepted design as in wind energy. The three main categories of WECs include oscillating water column, overtopping devices, and oscillating bodies.

Oscillating body WECs contain at least one moving body that is driven by the wave motion. The oscillating motion is converted into useful power using a power takeoff (PTO) system, which is typically either a hydraulic system or electric generator [5]. Oscillating body WECs generally fall into three classes: heaving, surging, or pitching. Heaving devices, or point absorbers, use bodies that float on the surface of the waves and contain a translational PTO system that is activated as the ocean waves cause movement in the vertical direction. Surging WECs, either bottom hinged or floating, take advantage of the wave motion in the horizontal direction. Pitching devices, on the other hand, use relative rotation between two or more bodies to produce power [6].

Pitching devices are further classified as either bottom-hinged or floating, also known as attenuators. Attenuators contain a series of sections linked with flexible joints that allow the sections to pitch relative to each other. The device is moored to the seafloor and placed along with the wave direction so that there is oscillation with the wave amplitude [7]. A number of different attenuators have been developed and tested, but much of the work has focused on large-scale power generation, including the McCabe Wave Pump, 750-1000 kW Pelamis, 500-6000 kW Wave Star, 375 kW Salter Duck, and 1000 kW Anaconda [8]. Analysis of large-scale attenuators and floating two-body devices has been performed in literature such as Ref. [9], [10], [11], [12], [13], and [14].

Increasingly, there is also interest in wave energy conversion at the small scale in addition to large scale

applications. There are numerous low-energy marine devices that could potentially be powered by ocean wave energy, such as navigation signs, illumination, sensors, survival kits, and electronics charging [15][16]. The U.S. Department of Energy (DOE) highlights the importance of small-scale ocean wave energy in the Powering the Blue Economy report [16]. The DOE has sponsored development of small-sized wave energy devices through design competitions including the Waves to Water competition focusing on wave-powered desalination and the Ocean Observing competition focusing on wave-powered devices for monitoring ocean conditions [17][18].

Power maximization and natural frequency tuning for a small-sized attenuator are more challenging than for large-sized devices. Many wave energy converters target a wave period of 5-12 seconds based on real ocean conditions [9][12][13][14], but it is difficult to achieve a resonant period high enough to be in that range with small-sized devices. Large-sized devices can use large overall dimensions and physical or added mass to adjust the natural frequency and increase the power [9][12][13][14]. However, using such large dimensions and mass is not possible with small-sized attenuators because of portability constraints. An innovative method for frequency tuning of small-sized attenuators is presented in this study through use of a thin tuning plate attached to each body.

The objective of this study is to develop a method of power maximization for a small-sized, two-body attenuator through resonance tuning and numerical simulation. The study first optimizes the geometry of the wave energy converter with a frequency domain method to match the natural frequency of the system with that of the incoming wave. The hydrodynamic coefficients are calculated with ANSYS AQWA. The study then adopts time domain simulation, using open-source tool WEC-Sim to optimize the PTO damping coefficient and power generation. The time domain simulation enables us to more realistically consider the influences of drag damping, various cross-section shapes, and mooring stiffness. Conclusions are drawn in Section 4.

2. MATERIALS AND METHODS 2.1 Design and Working Principle

In this study, the device under consideration is a small-sized, easily portable, two-body attenuator with a power takeoff around the hinge between the two bodies, as shown in Figure 1. The size is such that the device could be easily transported in the back of a car or other vehicle and carried by one or two people to be deployed in the ocean. The two main bodies could be disconnected and the thin plates folded to ease transportation, as shown in Figure 2. Without the tuning plate, the length of each main body is 0.5 m, so the overall length of the device without the plates will be about 1 m.

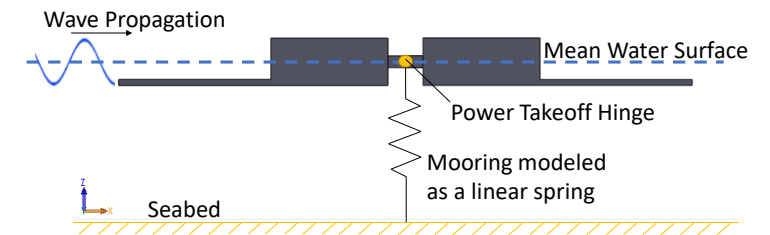


FIGURE 1: CONCEPT DIAGRAM FOR TWO-BODY ATTENUATOR

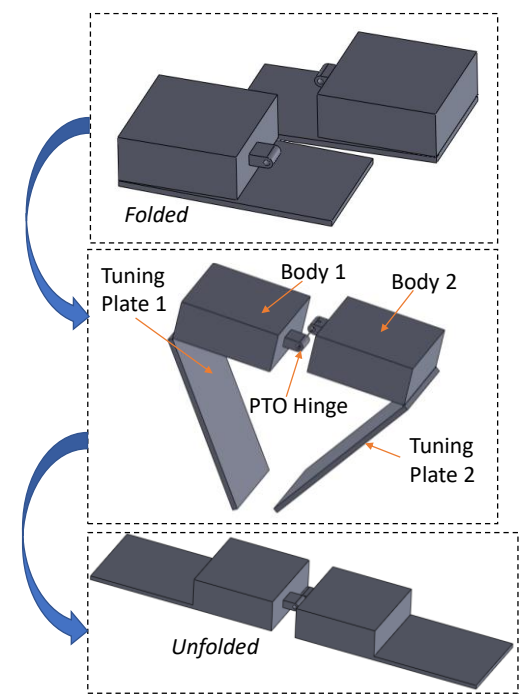


FIGURE 2: POSSIBLE SYSTEM DISASSEMBLY FOR TRANSPORT

2.2 System Governing Equations

In order to tune the two-body device to achieve resonance by matching the device natural frequency to the wave frequency, the equations of motion of the system were first derived. The equations defined in this section (Section 2.2) were used for dimensional optimization through natural frequency tuning while the equations and models shown in Section 2.4 were used to determine the time domain results. The two-degree-of-freedom (2DOF) system simplifies the device so that each body has one DOF in rotation around the hinge point (fixed), resulting in a 2DOF overall system, as illustrated in Figure 3. The 3DOF system allows the hinge to move in the heave direction with a mooring stiffness, as shown in Figure 4.

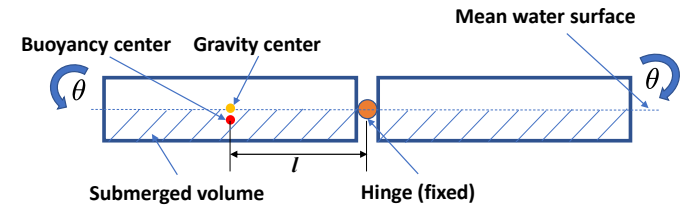


FIGURE 3: 2DOF MOTION SCHEMATIC OF THE ATTENUATOR WEC

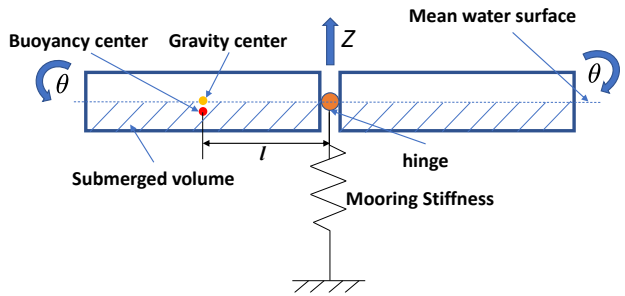


FIGURE 4: 3DOF MOTION SCHEMATIC OF THE ATTENUATOR WEC

Taking the sum of the moments for the system around the hinge point, equations are derived that are applicable to both the 2DOF and 3DOF systems. The overall equation of motion for the system is given by Equation 1, where J is the rotational inertia matrix with respect to the PTO hinge, $A(\omega)$ is the added rotational inertia with respect to the PTO at frequency ω , $C(\omega)$ is the PTO damping matrix, K is the hydrostatic stiffness matrix, M is the excitation moment vector, and θ , $\dot{\theta}$, and $\ddot{\theta}$ are the angular displacement, velocity, and acceleration respectively. The expanded matrices are shown in Equation 2.

$$(J + A(\omega))\ddot{\theta} + C(\omega)\dot{\theta} + K\theta = M$$

$$J = \begin{bmatrix} J_1 & 0 \\ 0 & J_2 \end{bmatrix}, \quad A(\omega) = \begin{bmatrix} A_1(\omega) & 0 \\ 0 & A_2(\omega) \end{bmatrix},$$

$$C(\omega) = \begin{bmatrix} c & -c \\ -c & c \end{bmatrix}, \quad K = \begin{bmatrix} k & 0 \\ 0 & k \end{bmatrix}$$
 (2)

We determine the hydrostatic stiffness of the two bodies with the following procedure. At hydrostatic equilibrium, the vertical summation of the forces gives Equation 3, where m is the body mass, g is acceleration due to gravity, ρ is the water density, and V_0 is the submerged volume with zero flap rotation.

$$mg = \rho g V_0 \tag{3}$$

By taking the sum of the moments for the individual body around the hinge point, we obtain Equation 4 where R_m is the hydrostatic moment on one body with respect to the PTO hinge and V_{θ} is the submerged volume. Note that V_{θ} is expanded around $\theta = 0$ using a Taylor series where k_1, k_2, \ldots are the coefficients of the Taylor series.

$$R_m = mglcos\theta - \rho gV_{\theta}lcos\theta$$

= $mglcos\theta - \rho g(V_0 + k_1\theta + k_2\theta^2 + \cdots)lcos\theta$ (4)

By taking the derivative of Equation 4 with respect to θ , we have Equation 5, i.e., the stiffness equals to the rate of the change of moment R_m at $\theta=0$. It is shown that the individual body stiffness is a function of the body's rate of change in volume with respect to θ , as shown in Equation 6. By calculating k_1 numerically, for example with a computer-aided design software, we are able to determine the rotational hydrostatic stiffness of the two bodies of an arbitrary shape.

$$-k = \frac{\partial R_m}{\partial \theta} |_{\theta=0}$$

$$= -mglsin\theta - \rho g(k_1 + 2k_2\theta + \cdots)lcos\theta + \rho g(V_0 + k_1\theta + k_2\theta^2 + \cdots)lsin\theta |_{\theta=0} = -\rho gk_1l$$
 (5)

$$k_1 = \frac{\partial V_{\theta}}{\partial \theta} |_{\theta=0} \tag{6}$$

Equation 7 gives the undamped natural frequency for one of the bodies. In the case of the attenuator, as a hydrodynamic system, the spring stiffness can be replaced by the body's hydrostatic stiffness and the mass becomes the sum of the inertia due to the body's dry material J_M and inertia due to added mass when submerged J_A . The natural period can be calculated using Equation 8.

$$\omega_n = \sqrt{\frac{k}{J_M + J_A}} \tag{7}$$

$$T_n = \frac{2\pi}{\omega_n} \tag{8}$$

2.3 Frequency Domain Natural Frequency Tuning

In order to maximize power absorption and achieve resonance, the natural frequency of each body was tuned to match the wave frequency. The target wave period was 6 seconds based on common wave conditions on the US east coast [17]. The dry material inertia J_M was obtained from the CAD model. The boundary element method (BEM) solver ANSYS AQWA was used to perform a hydrodynamic diffraction solution in the frequency domain to obtain J_A and k in order to use Equation 7 [19]. Because of the portability constraint, it was necessary to keep the overall body dimensions approximately close to the target overall system dimensions shown in Figure 5.

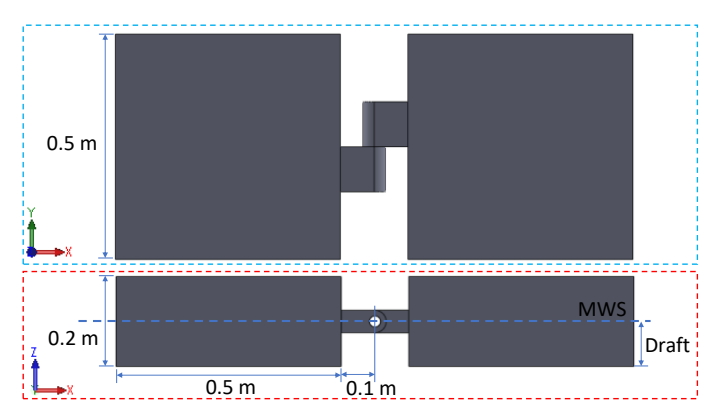


FIGURE 5: DESIRED OVERALL DIMENSION CONSTRAINTS FOR TWO-BODY ATTENUATOR

Table 1(a) shows a sample of geometry parameters and results for the baseline shape, a rectangular flat plate. As shown in Table 1(b), it is difficult to achieve a natural period much larger than 1 second because the hydrostatic stiffness k remained large relative to J_M and J_A . An intuitive modification is to increase the buoy length in order to achieve an increased added mass. However, as shown in Case 7 in Table 1, J_M and J_A were greatly increased from the initial case when increasing the buoy length, but hydrostatic stiffness also increased significantly, preventing the natural frequency from matching the targeted wave frequency.

TABLE 1(a): SAMPLE OF GEOMETRY VARIATION AND NATURAL FREQUENCY RESULTS FOR BASELINE SHAPE

	Variable Parameters						
				Buoy	Lever		
	Draft	Thickness	Width	Length	Length		
Case #	(m)	(m)	(m)	(m)	(m)		
1 (initial)	0.15	0.2	0.50	0.5	0.075		
2	0.10	0.2	0.50	0.5	0.075		
3	0.25	0.3	0.50	0.5	0.075		
4	0.15	0.2	0.75	0.5	0.075		
5	0.15	0.2	0.50	0.5	0.150		
6	0.15	0.2	0.50	0.5	0.500		
7	0.15	0.2	0.50	1.0	0.075		
8	0.45	0.5	0.50	0.5	0.075		

TABLE 1(b): SAMPLE OF GEOMETRY VARIATION AND NATURAL FREQUENCY RESULTS FOR BASELINE SHAPE

	Results						
Case #	K (N- m/rad)	J_M (kg*m^2)	J_A (kg.m²/rad)	wn (rad/s)	Tn (s)		
1 (initial)	308.36	1.11	6.27	6.64	0.97		
2	305.34	0.74	6.39	6.54	0.96		
3	302.08	2.00	6.10	6.11	1.03		
4	462.54	1.81	11.35	5.93	1.06		
5	445.00	1.15	9.24	6.55	0.96		
6	1456.47	6.61	32.11	6.13	1.02		
7	2061.67	7.19	56.73	5.68	1.11		
8	289.51	4.93	5.35	5.31	1.18		

After tuning the device using traditional geometry proved inadequate, a new geometry feature was added to make tuning possible. By adding a thin, submerged flat plate to the existing shape, it was possible to greatly increase the added mass without significantly increasing the hydrostatic stiffness. The body dimensions could be kept at the target values and the plate length varied to tune the body to the wave frequency, as shown in Figure 6. Using the tuning plate, the natural periods for the three different body shapes were tuned to approximately 6 s, as shown in Table 2.

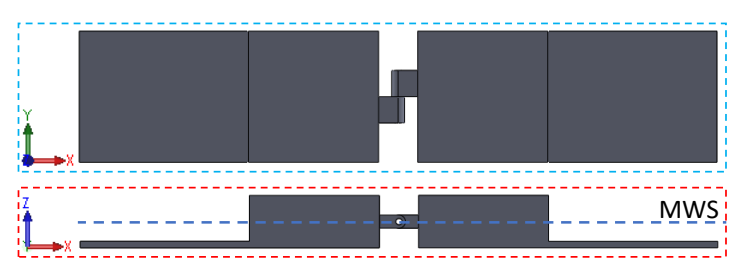


FIGURE 6: TWO-BODY ATTENUATOR WITH THIN TUNING PLATE

TABLE 2: TUNED NATURAL FREQUENCY FOR EACH SHAPE

	Thin Plate Length	Body Density (kg/	K (N- m	J_M (kg*	J_A (kg.m²/	wn (rad/	Tn
Shape	(m)	m^3)	/rad)	m^2)	rad)	s)	(s)
Rectangular	0.90	606	338	2.52	299	1.06	5.93
Elliptical	0.95	627	342	1.78	320	1.03	6.09
Quadrilateral	0.95	675	346	2.29	321	1.04	6.06

Three different body cross sections were used for the analysis, as shown in Figure 7: rectangular, elliptical, and quadrilateral. The shapes were chosen based on commonly studied cross sections found in literature such as Ref. [9] and [10]. The overall body dimensions were kept the same as those shown in Figure 5. A draft of 0.1 m was used for each body so that the mean water surface was in the center of the cross section. Reducing the draft would increase portability by reducing the body weight because as Equation 3 shows, body weight is proportional to displaced volume. However, for tapered shapes like the elliptical and quadrilateral, reducing the draft would also reduce the submerged body width. Excitation force decreases as submerged body width decreases because less of the body is exposed to the incoming wave front, leading to a reduction in power absorption. Consequently, the study is a fairer comparison if the submerged widths are same for the three geometries.

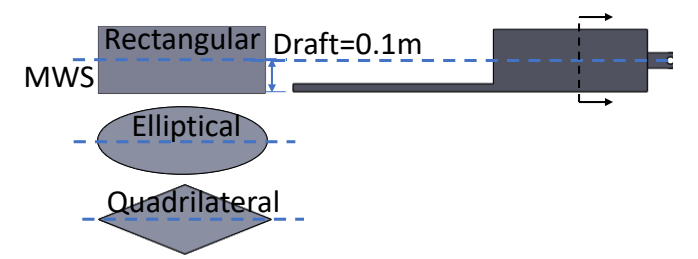


FIGURE 7: BODY CROSS SECTIONS USED FOR ANALYSIS

2.4 Time Domain Power Absorption Simulation

Power absorption modelling was performed using WEC-Sim, an open-source code created in MATLAB/Simulink by the National Renewable Energy Lab (NREL) for wave energy converter simulation [11]. A time-domain numerical model was created in WEC-Sim to solve the system dynamics. Initially, the simplified 2DOF model was used followed by the more realistic 3DOF model. In the WEC-Sim software, the dynamic response is calculated by solving the equation of motion for each body around its center of gravity using Equation 9, where M is the mass matrix, \ddot{X} is the (translational and rotational) acceleration vector of the body, $F_{exc}(t)$ is the wave excitation force and torque vector, $F_{rad}(t)$ is the force and torque vector resulting from wave radiation, $F_{pto}(t)$ is the PTO force and torque vector, $F_{\nu}(t)$ is the damping force and torque vector, $F_B(t)$ is the net buoyancy restoring force and torque vector, and $F_m(t)$ is the force and torque vector resulting from mooring connection [20]. Equation 9 was used to determine the time-domain results while the equations in Section 2.2 were only used for dimensional optimization.

$$M\ddot{X} = F_{exc}(t) + F_{rad}(t) + F_{pto}(t) + F_{v}(t) + F_{B}(t) + F_{m}(t)$$
(9)

Figure 8 shows the Simulink model of the 2-body attenuator for the 2DOF model. The two rigid bodies are constrained to rotate around a fixed center point using a rotational constraint. Heaving motion is not included in the 2DOF model, as if the center point is attached to a fixed structure. The rotational PTO captures power based on the relative rotational velocity between the two bodies according to Equation 10 where c is the PTO rotational damping and $\dot{\theta}_{rel}$ is the relative rotational velocity. PTO damping is assumed to be constant with respect to the relative rotational velocity between the two bodies.

$$P = c\dot{\theta}_{rel}^2 \tag{10}$$

In each 2DOF simulation case, there was a ramp time of $150 \, \mathrm{s}$ and time step of $0.05 \, \mathrm{s}$. The solver ode4 was used with the fixed time step. Regular wave simulations used a duration of $500 \, \mathrm{s}$ while irregular wave simulations used a duration of $750 \, \mathrm{s}$ to provide additional simulation data for taking the average power because power fluctuates more under irregular waves due to the

wave spectrum. Average power was calculated from the instantaneous PTO power after the simulation reached steady state. A wave period of T=6 s and wave height of H=0.5 m was used for each case. Assuming that the two-body attenuator would be deployed close to shore, a water depth of 5 m was used. In order to study the effects of drag, four different drag coefficients of Cd=0.5, 1, 1.5, 2 were used in calculation F_{ν} . These four drag coefficients were determined to be in the reasonable range for the WEC type and body shapes based on literature such as Ref. [21] and [22].

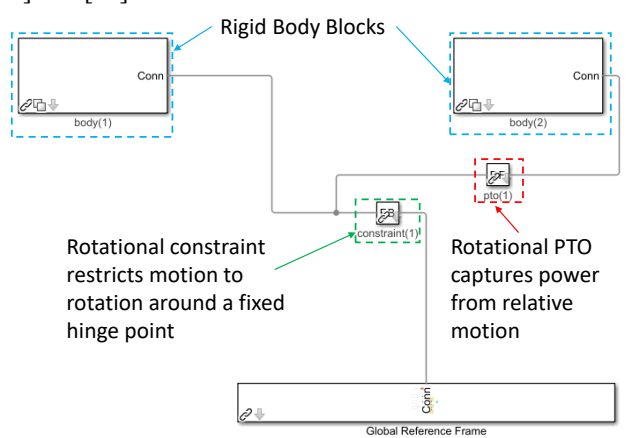


FIGURE 8: SIMULINK MODEL OF THE 2DOF SYSTEM

To obtain the max power and optimal damping for each cross section and Cd, WEC-Sim's multiple condition run (MCR) feature was used to run a series of cases with different rotational damping values. For each cross section, each Cd was simulated with rotational damping from 0-500 Nsm/rad with a step of 10 Nsm/rad, or in other words, 50 cases for each Cd.

Wave energy flux, J_p , is the mean power per wave front width available in the wave. It can be calculated using Equation 11, where ρ is the water density, g is acceleration due to gravity, T is wave height, and H is wave period [23]. Capture width (CW) is the amount of wave crest width that is completely captured and absorbed by the WEC. It is calculated according to Equation 12 by taking the ratio of average absorbed wave power P_{avg} to wave energy flux J. As a non-dimensional way to quantify the hydrodynamic efficiency, the capture width ratio CWR was calculated using Equation 13 by dividing the capture width (CW) by the device characteristic dimension L [24]. In the case of the two-body attenuator, the characteristic dimension is the device submerged width of 0.5 m, which is perpendicular to the incoming wave front.

$$J_p = \frac{\rho g^2 T H^2}{64\pi} \tag{11}$$

$$CW = P_{ava}/J_p \tag{12}$$

$$CWR = CW/L \tag{13}$$

After simulations were performed with the 2DOF model, a 3DOF model that accounts for the WEC heave motion was used.

The 3DOF model is shown in Figure 9. To allow the device to heave up and down, a non-hydro body was connected to the seabed using a translational constraint. The non-hydro body has no hydrodynamic interaction in the model and is only used to enable the heave motion. Two rotational PTOs are connected between the side bodies and non-hydro body, allowing the side bodies to pitch around the non-hydro body. For each case, the two PTO damping values were set equal. To simulate a single mooring line attached to the WEC center point, a mooring stiffness acting in the heave direction was added to the non-hydro body. Power absorption was calculated using Equation 10 based on the relative velocity of the two side bodies.

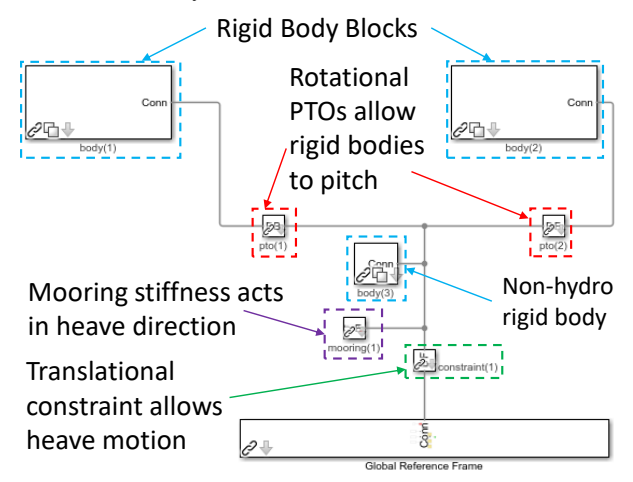


FIGURE 9: SIMULINK MODEL OF THE 3DOF SYSTEM

Using the 3DOF model, two different studies were performed: a drag study and mooring stiffness study. The 3DOF model used the same wave period, wave height, and water depth as the 2DOF model. The same ramp time and simulation duration were also used. The drag study was performed with the same four drag coefficients. For the drag study, a baseline value for the mooring stiffness $k_{mooring}$ was used by setting $k_{mooring}$ equal to the combined heave hydrostatic stiffness $k_{hydrostatic}$ of the side bodies. The hydrostatic stiffness was obtained from AQWA, leading to a baseline mooring stiffness of 5277.2 N/m, the same for all three cross section geometries. Because of the increased system stiffness due to the mooring, a smaller time step of 0.025 s was necessary. As with the 2DOF model, each drag coefficient had a rotational damping range of 0-500 Nsm/rad with a time step of 10 Nsm/rad, leading to 50 cases for each drag coefficient. For the mooring stiffness study, a series of different mooring stiffness values with respect to the hydrostatic stiffness were used. Regular waves were used for the mooring stiffness study. Like the drag study, rotational damping was varied from 0-500 Nsm/rad with a step of 10 Nsm/rad.

3. RESULTS AND DISCUSSION 3.1 Two DOF Results

Figures 10, 11, and 12 show the 2DOF regular and irregular wave power absorption results under different drag coefficients for the three shapes. Table 3 summarizes the 2DOF results for

optimal damping, maximum power, and capture width ratio. Out of all the shapes and drag coefficients, maximum power occurred with rotational damping of 80-160 Nsm/rad. The rectangular shape with Cd 0.5 had the largest max power of the different shapes and drag coefficients: 37.33 W with CWR of 10.15% for regular waves and 11.03 W with 3.00% CWR for irregular waves. There is not a significant difference in power absorption between the shapes for a given drag coefficient. The small difference is logical because submerged body widths are equal for each shape, so for the same drag coefficient, excitation forces and power absorbed are expected to be similar.

TABLE 3: 2DOF POWER RESULTS SUMMARY

		Rectangular								
	Reg	ular Wave	<u> </u>	Irreg	ular Wave	!				
Cd	C_opt (Nsm/rad)	P_max (W)	CWR	C_opt (Nsm/rad)	P_max (W)	CWR				
0.5	80	37.33	10.15%	80	11.03	3.00%				
1.0	110	30.28	8.23%	110	9.02	2.45%				
1.5	130	26.07	7.09%	130	7.89	2.15%				
2.0	150	23.16	6.29%	150	7.13	1.94%				

		Elliptical							
	Reg	ular Wave		Irreg	Irregular Wave				
	C_opt	P_max		C_opt	P_max				
<u>Cd</u>	(Nsm/rad)	(W)	CWR	(Nsm/rad)	(W)	CWR			
0.5	90	33.51	9.11%	120	10.15	2.76%			
1.0	120	27.09	7.36%	150	8.32	2.26%			
1.5	140	23.40	6.36%	170	7.29	1.98%			
2.0	160	20.82	5.66%	190	6.60	1.79%			

		Quadrilateral								
	Reg	Regular Wave			Irregular Wave					
	C_opt	P_max		-	C_opt	P_max				
Cd	(Nsm/rad)	(W)	CWR		(Nsm/rad)	(W)	CWR			
0.5	90	32.50	8.83%		120	10.22	2.78%			
1.0	120	27.12	7.37%		150	8.47	2.30%			
1.5	140	23.71	6.44%		170	7.45	2.02%			
2.0	160	21.20	5.76%		190	6.75	1.83%			

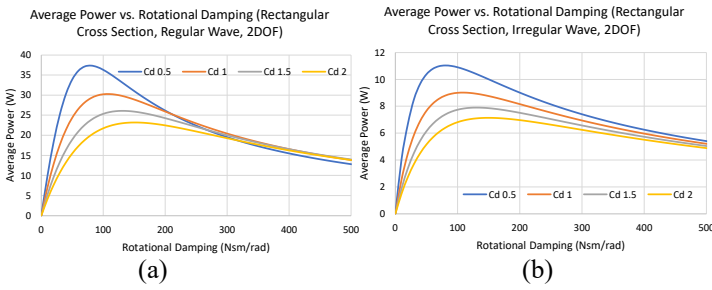


FIGURE 10: 2DOF POWER RESULTS, RECTANGULAR CROSS SECTION

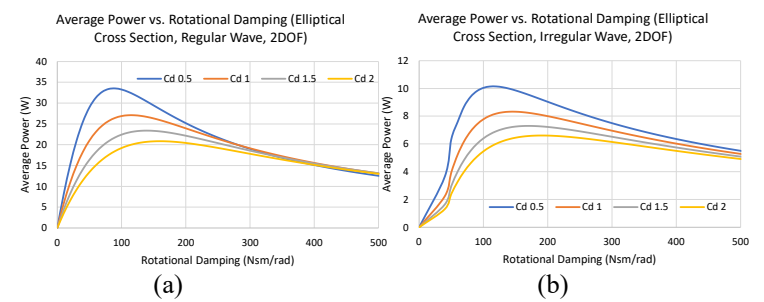


FIGURE 11: 2DOF POWER RESULTS, ELLIPTICAL CROSS SECTION

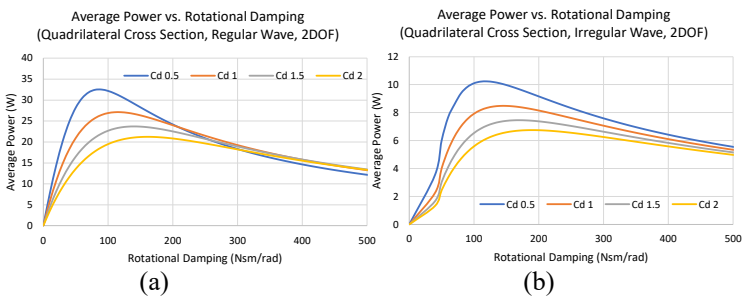


FIGURE 12: 2DOF POWER RESULTS, QUADRILATERAL CROSS SECTION

When rotational damping becomes large, the two bodies tend to rotate together as one, causing small relative motion and therefore small power extracted by the PTO. Figures 13 and 14 illustrate this effect. The rotational velocity is out of phase for smaller damping values such as 80 Nsm/rad and nearly in phase for large damping values like 1000 Nsm/rad.

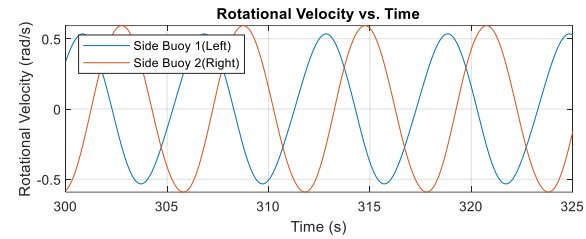


FIGURE 13: ROTATIONAL VELOCITY, RECTANGULAR CROSS SECTION, 80 Nsm/rad DAMPING, 0.5 Cd, REGULAR WAVE

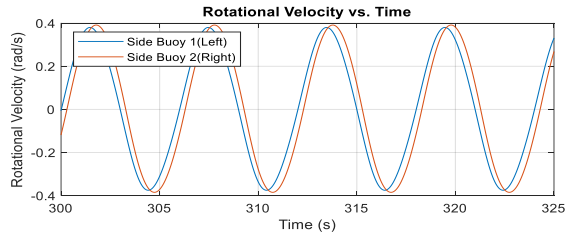


FIGURE 14: ROTATIONAL VELOCITY, RECTANGULAR CROSS SECTION, 1000 Nsm/rad DAMPING, 0.5 Cd, REGULAR WAVE

In reality, tapered cross section geometries like the elliptical and quadrilateral shapes would have lower drag coefficients. One possible comparison is to choose an approximate drag coefficient for each shape out of the four Cd values used for the study, such as Cd=1 for the elliptical shape, Cd=1.5 for the quadrilateral, and Cd=2 for the rectangular [22]. Figure 15 shows this comparison. Using approximate drag coefficients, the elliptical shape would have the highest power absorption of 27.09 W with 7.36% CWR at 120 Nsm/rad optimal damping for regular waves and 8.32 W with 2.26% CWR at 150 Nsm/rad optimal damping for irregular waves.

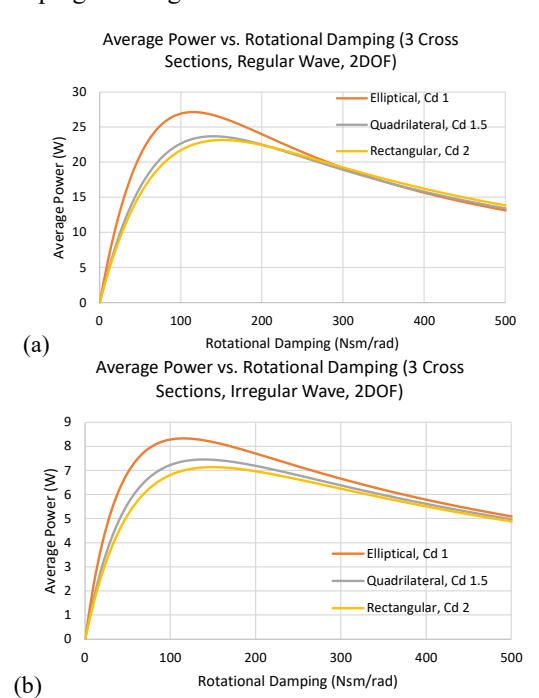


FIGURE 15: 2DOF POWER RESULTS COMPARISON WITH APPROXIMATE DRAG COEFFICIENTS

3.2 Three DOF Drag Study Results

Figures 16, 17, and 18 show the 3DOF drag study results. Table 4 summarizes the 3DOF results for optimal damping, maximum power, and capture width ratio. The optimal damping ranged from 160-380 Nsm/rad. Like the 2DOF study, the rectangular shape with Cd 0.5 had the highest max power out of the different shapes and drag coefficients: 33.04 W with 8.98% CWR for regular waves and 8.51 W with 2.31% CWR for irregular waves. As with the 2DOF study, the difference in power between the shapes is small for the same drag coefficient, which is expected because the three shapes have the same submerged body width.

TABLE 4: 3DOF DRAG STUDY POWER RESULTS SUMMARY

	Rectangular							
	Re	egular Wa	ve	Irr	Irregular Wave			
	C_opt (Nsm/	P_max		C_opt (Nsm/	P_max			
Cd	rad)	(W)	CWR	rad)	(W)	CWR		
0.5	160	33.04	8.98%	130	8.51	2.31%		
1.0	200	25.61	6.96%	200	6.82	1.85%		
1.5	230	21.48	5.84%	260	6.00	1.63%		
2.0	260	18.81	5.11%	320	5.50	1.50%		

		Elliptical									
	Re	gular Wa	ve	Irr	egular Wa	ve					
	C_opt (Nsm/	P_max		C_opt (Nsm/	P_max						
Cd	rad)	(W)	CWR	rad)	(W)	CWR					
0.5	180	28.65	7.79%	150	7.60	2.07%					
1.0	210	22.52	6.12%	230	6.18	1.68%					
1.5	250	19.00	5.16%	310	5.51	1.50%					
2.0	280	16.68	4.53%	390	5.10	1.39%					

		Quadrilateral						
	Re	Regular Wave			egular Wa	ve		
	C_opt (Nsm/	P_max		C_opt (Nsm/	P_max			
Cd	rad)	(W)	CWR	rad)	(W)	CWR		
0.5	180	28.59	7.77%	150	7.59	2.06%		
1.0	220	22.46	6.10%	240	6.16	1.67%		
1.5	260	18.94	5.15%	310	5.48	1.49%		
2.0	290	16.62	4.52%	380	5.06	1.37%		

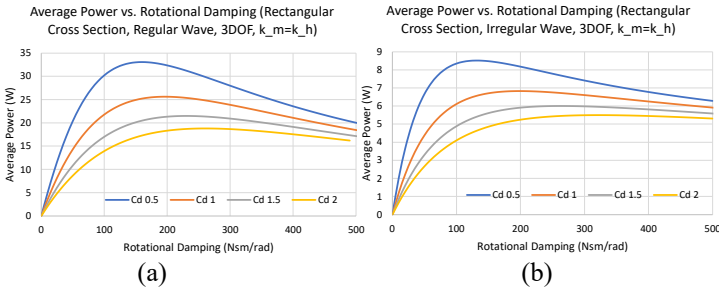


FIGURE 16: 3DOF POWER RESULTS, RECTANGULAR CROSS SECTION

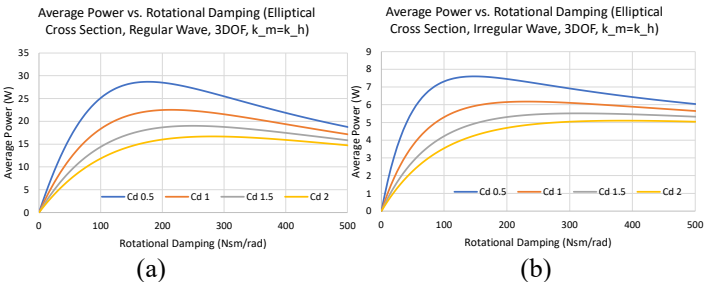


FIGURE 17: 3DOF POWER RESULTS, ELLIPTICAL CROSS SECTION

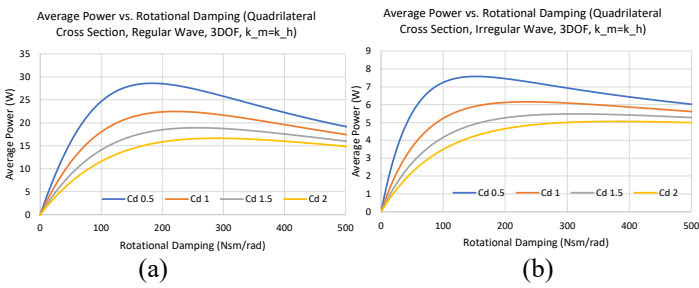


FIGURE 18: 3DOF POWER RESULTS, QUADRILATERAL CROSS SECTION

As with the 2DOF study, an approximate drag coefficient can be used to compare the 3DOF drag study results, as shown in Figure 19. Based on this comparison, the elliptical shape would have the highest power absorption of 22.52 W with 6.12% CWR at 210 Nsm/rad optimal damping for regular waves and 6.18 W with 1.68% CWR at 230 Nsm/rad optimal damping for irregular waves. This comparison agrees with the 2DOF comparison with approximate drag coefficients, which also showed the elliptical shape to have the highest power.

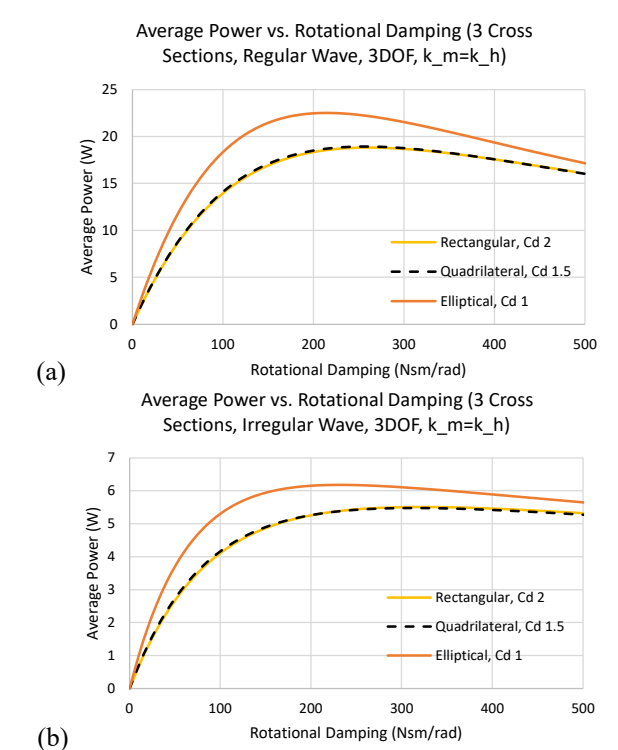


FIGURE 18: 3DOF POWER RESULTS COMPARISON WITH APPROXIMATE DRAG COEFFICIENTS

3.3 Three DOF Mooring Study Results

The 3DOF mooring stiffness results for the three different shapes are shown in Figure 20. Table 5 summarizes the mooring stiffness power results. For low mooring stiffness values like the $k_{mooring}=k_{hydrostatic}*0.1$ case, there is no significant difference in power between the three shapes. With higher mooring stiffnesses such as $k_{mooring}=k_{hydrostatic}$ and larger, the elliptical shape had the highest power absorption when using the approximate drag coefficients. The mooring stiffness study demonstrated that increased mooring stiffness can be used to increase relative motion between the two bodies in order to increase the power. The mooring stiffness study can be applied to different WEC types, geometries, and sizes.

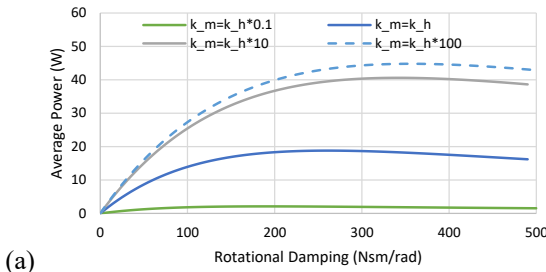
TABLE 5: 3DOF MOORING STUDY RESULTS SUMMARY

	Rectangular (Cd 2)				
k_m (N/m)	C_opt (Nsm/rad)	P_max (W)	CWR		
k_m=k_h*0.1	190	2.07	0.56%		
k_m=k_h	260	18.81	5.11%		
k_m=k_h*10	340	40.52	11.01%		
km=k_h*100	360	44.72	12.15%		

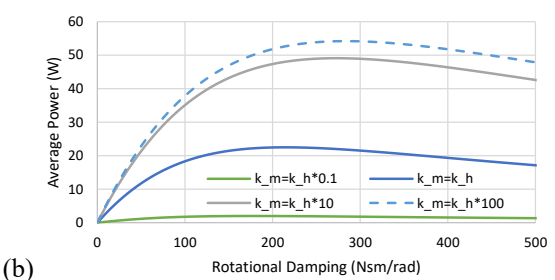
	Elliptical (Cd 1)				
k_m (N/m)	C_opt (Nsm/rad)	P_max (W)	CWR		
k_m=k_h*0.1	180	1.97	0.54%		
k_m=k_h	210	22.52	6.12%		
k_m=k_h*10	270	49.07	13.34%		
_km=k_h*100	280	54.22	14.74%		

	Quadrilateral (Cd 1.5)					
k_m (N/m)	C_opt (Nsm/rad)	P_max (W)	CWR			
k_m=k_h*0.1	200	2.15	0.58%			
k_m=k_h	260	18.94	5.15%			
k_m=k_h*10	340	40.64	11.05%			
km=k_h*100	350	44.82	12.18%			

Average Power vs. Rotational Damping (Rectangular Cross Section, Regular Wave, 3DOF, Cd 2)



Average Power vs. Rotational Damping (Elliptical Cross Section, Regular Wave, 3DOF, Cd 1)



Average Power vs. Rotational Damping (Quadrilateral Cross Section, Regular Wave, 3DOF, Cd 1.5)

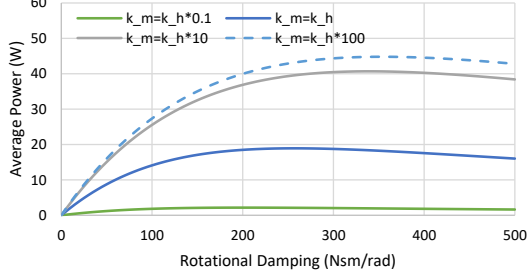


FIGURE 20: 3DOF MOORING STIFFNESS STUDY RESULTS

(c)

4. CONCLUSION

When tuning the natural frequency of the small-scale device to the wave frequency, a major challenge was the small material and added inertias (or masses) relative to the hydrostatic stiffness. To overcome this issue, we propose to use a thin, submerged plate to increase added mass without greatly increasing stiffness. Three typical cross section shapes of the same overall dimension constraint were compared: rectangular. elliptical, and quadrilateral. When variation in drag between the three shapes was not considered, there was not a significant difference in power absorption between the shapes. If an approximate drag coefficient was assigned to each shape, then the elliptical shape had the highest power. Using the approximate drag coefficient comparison for the 2DOF model, the elliptical shape had a max power of 27.09 W with 7.36% CWR for regular waves and a max power of 8.32 W with 2.26% CWR for irregular waves. Using the approximate drag coefficient comparison for the 3DOF model, the elliptical cross section had a max power of 22.52 W with 6.12% CWR for regular waves and 6.18 W with 1.68% CWR for irregular waves. The mooring stiffness study showed that increasing mooring stiffness can be used to increase power by increasing relative motion between the bodies. For low mooring stiffness values, there was not a significant difference in the results between the different shapes, but the elliptical shape had the highest power for larger mooring stiffness values when using approximate drag coefficients.

ACKNOWLEDGEMENTS

The material in this paper is based on work supported by the US Environmental Protection Agency under Grant No. EPA 83991001-0.

REFERENCES

- [1] Mafi-Gholami, D., Jaafari, A., Zenner, E. K., Kamari, A. N., & Bui, D. T. (2020). Vulnerability of coastal communities to climate change: Thirty-year trend analysis and prospective prediction for the coastal regions of the Persian Gulf and Gulf of Oman. Science of the Total Environment, 741, 140305.
- [2] Huckerby, John, Henry Jeffrey, and Brighid Jay. "An International Vision for Ocean Energy (Phase 1)." (2011).
- [3] Vosough, Amir. "Wave energy." *International journal of multidisciplinary sciences and engineering* 2, no. 7 (2011): 60-63.
- [4] Jacobson, Paul T., George Hagerman, and George Scott. *Mapping and assessment of the United States ocean wave energy resource*. No. DOE/GO/18173-1. Electric Power Research Institute, 2011.
- [5] António, F. de O. "Modelling and control of oscillating-body wave energy converters with hydraulic power take-off and gas accumulator." *Ocean engineering* 34, no. 14-15 (2007): 2021-2032.
- [6] Prakash, S. S., K. A. Mamun, F. R. Islam, Rishaal Mudliar, Cherie Pau'u, Manasa Kolivuso, and Semi Cadralala. "Wave energy converter: a review of wave energy conversion technology." In 2016 3rd Asia-Pacific World Congress on

- Computer Science and Engineering (APWC on CSE), pp. 71-77. IEEE, 2016.
- [7] López, Iraide, Jon Andreu, Salvador Ceballos, Iñigo Martínez De Alegría, and Iñigo Kortabarria. "Review of wave energy technologies and the necessary power-equipment." *Renewable and sustainable energy reviews* 27 (2013): 413-434.
- [8] Alamian, Rezvan, Rouzbeh Shafaghat, S. Jalal Miri, Nima Yazdanshenas, and Mostafa Shakeri. "Evaluation of technologies for harvesting wave energy in Caspian Sea." *Renewable and sustainable energy reviews* 32 (2014): 468-476.
- [9] Zheng, Si-Ming, Yong-Hao Zhang, Yong-Liang Zhang, and Wan-An Sheng. "Numerical study on the dynamics of a two-raft wave energy conversion device." *Journal of Fluids and Structures* 58 (2015): 271-290.
- [10] Liu, ChangHai, QingJun Yang, and Gang Bao. "Performance investigation of a two-raft-type wave energy converter with hydraulic power take-off unit." *Applied Ocean Research* 62 (2017): 139-155.
- [11] So, Ratanak, Carlos Michelen, Bret Bosma, Pukha Lenee-Bluhm, and Ted KA Brekken. "Statistical analysis of a 1: 7 scale field test wave energy converter using WEC-sim." *IEEE Transactions on Sustainable Energy* 8, no. 3 (2017): 1118-1126.
- [12] Wang, L., and John V. Ringwood. "Geometric optimization of a hinge-barge wave energy converter." In *Proceedings of the 13th European Wave and Tidal Energy Conference, Naples, Italy*, pp. 1-6. 2019.
- [13] Li, Biao, Fangfang Sui, and Bingsong Yang. "An efficient multi-factor geometry optimization based on motion analysis and resonance response for hinged double-body floating wave energy converter." *Science Progress* 103, no. 3 (2020): 0036850420950151.
- [14] Li, Qiaofeng, Jia Mi, Xiaofan Li, Shuo Chen, Boxi Jiang, and Lei Zuo. "A self-floating oscillating surge wave energy converter." *Energy* (2021): 120668.
- [15] Blažauskas, Nerijus, Aleksas Pašilis, and Audrius Knolis. "Potential applications for small scale wave energy installations." *Renewable and Sustainable Energy Reviews* 49 (2015): 297-305.
- [16] LiVecchi, A., A. Copping, D. Jenne, A. Gorton, R. Preus, G. Gill, R. Robichaud et al. "Powering the blue economy; exploring opportunities for marine renewable energy in maritime markets." *US Department of Energy, Office of Energy Efficiency and Renewable Energy. Washington, DC* (2019): 207.
- [17] 2021, "American-Made Challenges: Waves to Water." from https://www.herox.com/wavestowater/guidelines
- [18] 2021, "American-Made Challenges: Ocean Observing Prize." from
- https://americanmadechallenges.org/oceanobserving/
- [19] 2020, "ANSYS AQWA 2020 R2 AQWA User's Manual."
- [20] WEC-Sim (Wave Energy Converter SIMulator). (2020). National Renewable Energy Laboratory (NREL) and Sandia National Laboratories.

- [21] Heras, Pilar, Sarah Thomas, Morten Kramer, and Jens Peter Kofoed. "Numerical and experimental modelling of a wave energy converter pitching in close proximity to a fixed structure." *Journal of Marine Science and Engineering* 7, no. 7 (2019): 218.
- [22] Hoerner, Sighard F. "Fluid-Dynamic Drag. Theoretical, experimental and statistical information." *Copyright by: SF Hoerner Fluid Dynamics, Vancouver, Printed in the USA, Card Number 64-19666* (1965).
- [23] Guillou, Nicolas. "Estimating wave energy flux from significant wave height and peak period." *Renewable Energy* 155 (2020): 1383-1393.
- [24] Babarit, Aurélien. "A database of capture width ratio of wave energy converters." *Renewable Energy* 80 (2015): 610-628.